Eur. Phys. J. A **31**, 273–278 (2007)
DOI 10.1140/epja/i2006-10224-4

THE EUROPEAN PHYSICAL JOURNAL A

Regular Article – Nuclear Structure and Reactions

Constrained relativistic mean-field approach with fixed configurations

H.F. Lü[1,2], L.S. Geng[1], and J. Meng[1,3,4,a]

[1] School of Physics, Peking University, Beijing 100871, PRC
[2] School of Science, Chinese Agriculture University, Beijing 100083, PRC
[3] Institute of Theoretical Physics, Chinese Academy of Sciences, Beijing 100080, PRC
[4] Center of Theoretical Nuclear Physics, National Laboratory of Heavy Ion Accelerator, Lanzhou 730000, PRC

Received: 29 May 2006 / Revised: 1 February 2007
Published online: 28 February 2007 –
Communicated by G. Orlandini

Abstract. A diabatic (configuration-fixed) constrained approach to calculate the potential energy surface (PES) of the nucleus is developed in the relativistic mean-field model. As an example, the potential energy surfaces of ^{208}Pb obtained from both adiabatic and diabatic constrained approaches are investigated and compared. It is shown that the diabatic constrained approach enables one to decompose the segmented PES obtained in usual adiabatic approaches into separate parts uniquely characterized by different configurations, to follow the evolution of single-particle orbits till the very deformed region, and to obtain several well-defined deformed excited states which can hardly be expected from the adiabatic PESs.

PACS. 21.10.Dr Binding energies and masses – 21.10.Re Collective levels – 21.60.Jz Hartree-Fock and random-phase approximations – 21.10.Pc Single-particle levels and strength functions

1 Introduction

The relativistic mean-field (RMF) theory is one of the most successful microscopic models in nuclear physics. The RMF theory incorporates from the beginning very important relativistic effects, such as the existence of two types of potentials (Lorentz scalar and four-vector) and the resulting strong spin-orbit interaction, a new saturation mechanism by the relativistic quenching of the attractive scalar field, and the existence of anti-particle solutions. The Lorentz covariance and special relativity make the RMF theory more appealing for studies of high-density and high-temperature nuclear matter [1–3]. It has achieved success in describing many nuclear phenomena for stable nuclei [2,3], exotic nuclei [4,5] as well as supernova and neutron stars [6]. The RMF theory provides a new explanation for the identical bands in superdeformed nuclei [7] and the neutron halo [4]; predicts a new phenomenon —giant neutron halos in heavy nuclei close to the neutron drip line [5,8]; gives naturally the spin-orbit potential, the origin of the pseudospin symmetry [9, 10] as a relativistic symmetry [11–13], and spin symmetry in the anti-nucleon spectrum [14], and well describes the magnetic rotation [15], the collective multipole excitations [16], and the properties of hypernuclei, etc. Lately, the ground-state properties of over 7000 nuclei have been calculated in the RMF+BCS model and good agreements with existing experimental data are obtained [17]. Recent and more complete reviews of the applications of the RMF model, particularly those on exotic nuclei, can be found in refs. [18,19].

In order to describe the shape of the atomic nucleus and understand the fusion and fission processes, it is crucial to obtain the potential energy surface (PES) of the nucleus as a function of the deformation [20]. In phenomenological methods, the PES is obtained by minimizing the total energy of the system with some shape parameters. In microscopic models, such as Skyrme-Hartree-Fock and RMF model, PES can be obtained in a constrained calculation. There are two different ways to obtain the PES, *i.e.*, adiabatic and configuration-fixed (diabatic) constrained approaches. In the adiabatic approach, one always occupies the orbital that results in the lowest configuration energy. However, the PES obtained in adiabatic calculations may correspond to different configurations wherever there is orbital crossing. To obtain the PES for a given configuration, the concept of the so-called "parallel transport" should be used, which enables one to decompose the ground state PES into separate parts uniquely characterized by the quantum numbers of the occupied orbits [21,22]. This configuration-fixed constrained approach is often referred to as the diabatic constrained approach in the literature [21–23].

[a] e-mail: mengj@pku.edu.cn

The diabatic constrained approach is useful to investigate level crossings which lead to flip-flop situations. It is also useful in the Generator-Coordinate-Method (GCM) calculations in cases that excited configurations are included. Although the so-obtained excited states cannot always be identified as physical states since the solutions of the corresponding equations violate the variational principle, the diabatic constrained approach may serve as a basis to qualitatively understand the excited states and the interplay between the excited states and the ground state. To describe these more quantitatively, one certainly should go beyond the mean-field level.

Conventionally, the diabatic constrained method has been combined with the non-relativistic approaches, such as shell model, Skyrme- or Gogny-Hartree-Fock or Hartree-Fock-Bogoliubov methods, in understanding the properties of atomic nuclei, including high-spin states [23], level crossings [24], fusion and fission processes [25], etc. For example, the interesting phenomenon of shape coexistence [26] can be studied using PES in complementary to the conventional interpretation of many-particle many-hole excitations [27]. In the RMF model, the diabatic constrained method has not received enough attention compared with that of the adiabatic constrained method and the non-relativistic ones. Therefore, the purpose of this paper is to develop the diabatic constrained approach within the RMF model and the doubly magic nucleus ^{208}Pb is chosen as an example for demonstration.

This paper is organized as follows: sect. 2 contains an outline of the RMF model. The adiabatic and diabatic constrained PES in ^{208}Pb, together with the diabatic single-particle spectra of the spherical ground state, are analyzed in sect. 3. The results are briefly summarized in sect. 4.

2 Theoretical framework

The relativistic mean-field model describes the nucleus as a system of Dirac nucleons which interact in a relativistic covariant manner via the meson fields. The meson fields considered in most applications of the RMF model are the scalar-isoscalar sigma meson, vector-isoscalar omega meson, vector-isovector rho meson and the photon: the sigma meson provides the long-range attractive interaction, the omega meson provides the short- and mid-range repulsive interaction, the rho meson is responsible for the isospin dependence of the nuclear force while the photon accounts for the electromagnetic interaction. The Lagrangian density used in our present calculation is of the following form:

$$\begin{aligned}\mathcal{L} = &\bar{\psi}\left(\not{p} - g_\omega \not{\omega} - g_\rho \not{\vec{\rho}}\vec{\tau} - \frac{1}{2}e(1-\tau_3)\not{A} - g_\sigma\sigma - m\right)\psi \\ &+\frac{1}{2}\partial_\mu\sigma\partial^\mu\sigma - \frac{1}{2}m_\sigma^2\sigma^2 - \frac{1}{3}g_2\sigma^3 - \frac{1}{4}g_3\sigma^4 \\ &-\frac{1}{4}\Omega_{\mu\nu}\Omega^{\mu\nu} + \frac{1}{2}m_\omega^2\omega_\mu\omega^\mu + \frac{1}{4}c_3(\omega_\mu\omega^\mu)^2 \\ &-\frac{1}{4}\vec{R}_{\mu\nu}\vec{R}^{\mu\nu} + \frac{1}{2}m_\rho^2\vec{\rho}_\mu\vec{\rho}^\mu - \frac{1}{4}F_{\mu\nu}F^{\mu\nu}, \end{aligned} \tag{1}$$

where ψ is the Dirac spinor and $\bar{\psi} = \psi^\dagger\gamma^0$. m, m_σ, m_ω, and m_ρ are the nucleon, σ, ω and ρ meson masses, respectively, while g_σ, g_2, g_3, g_ω, c_3, g_ρ, and $e^2/4\pi = 1/137$ are the corresponding coupling constants for the mesons and the photon. The field tensors of the vector mesons (ω and ρ) and of the electromagnetic fields take the following form:

$$\Omega^{\mu\nu} = \partial^\mu\omega^\nu - \partial^\nu\omega^\mu, \tag{2a}$$

$$\vec{R}^{\mu\nu} = \partial^\mu\vec{\rho}^\nu - \partial^\nu\vec{\rho}^\mu - 2g_\rho\vec{\rho}^\mu \times \vec{\rho}^\nu, \tag{2b}$$

$$F^{\mu\nu} = \partial^\mu A^\nu - \partial^\nu A^\mu. \tag{2c}$$

With the classical variational principle, one can obtain the coupled equations of motion, *i.e.*, the Dirac equation for the nucleons and the Klein-Gordon–type equations for the mesons and the photon. In the most general case, these equations are very difficult to solve; therefore various symmetries must be utilized to simplify them.

In the case of an axially symmetric system, the projection of the angular momentum on the z-axis, Ω, and the parity, π, are good quantum numbers. Here, we consider only even-even nuclei, therefore time reversal symmetry is conserved. To solve the RMF equations for an axially symmetric system, we expand the Dirac spinors and the Boson fields with the eigenfunctions of a deformed harmonic-oscillator potential in cylindrical coordinates [28], *i.e.*,

$$\begin{aligned}\psi_i(\vec{r},t) = &\begin{pmatrix} f_i(\vec{r}) \\ ig_i(\vec{r}) \end{pmatrix}\chi_{t_i}(t) = \\ &\frac{\chi_{t_i}(t)}{\sqrt{2\pi}}\begin{pmatrix} f_i^+(z,r_\perp)e^{i(\Omega_i-1/2)\theta} \\ f_i^-(z,r_\perp)e^{i(\Omega_i+1/2)\theta} \\ ig_i^+(z,r_\perp)e^{i(\Omega_i-1/2)\theta} \\ ig_i^-(z,r_\perp)e^{i(\Omega_i+1/2)\theta} \end{pmatrix}. \end{aligned} \tag{3}$$

In this paper, 20 oscillator shells have been used to expand both the Fermion fields and Boson fields to guarantee convergence.

The potential energy surface is obtained through the constrained calculation. More specifically, the binding energy at certain deformation is obtained by constraining the quadruple moment $\langle\hat{Q}_2\rangle$ to a given value μ, *i.e.*,

$$\langle H'\rangle = \langle H\rangle + \frac{1}{2}C(\langle\hat{Q}_2\rangle - \mu)^2, \tag{4}$$

with

$$\langle\hat{Q}_2\rangle = \langle\hat{Q}_2\rangle_n + \langle\hat{Q}_2\rangle_p, \tag{5}$$

where $\langle\hat{Q}_2\rangle_{n,p} = \langle 2r^2P_2(cos\theta)\rangle_{n,p} = \langle 2z^2 - x^2 - y^2\rangle_{n,p}$ and C is the curvature constant parameter. The more often used deformation parameter β_2 is related with the expectation value $\langle\hat{Q}_2\rangle$ by $\langle\hat{Q}_2\rangle = \frac{3}{\sqrt{5\pi}}Ar^2\beta_2$, $r = R_0A^{1/3}$ ($R_0 = 1.2\,\mathrm{fm}$) and A is the mass number. By varying μ, the binding energy at different deformation can be obtained. In principle, one has to follow a multidimensional energy surface. However, for the sake of efficiency, a one-parameter line, *e.g.* β_2, is often used in microscopic constrained RMF calculations due to the self-consistency [29]

and the small effects of other deformations, such as the hexadecupole deformation.

In order to obtain the diabatic PES with a fixed configuration, the occupied orbits are determined by the so-called "parallel transport", *i.e.*,

$$\langle\psi_i(q)|\psi_j(q+\Delta q)\rangle|_{\Delta q\to 0} \approx \delta_{ij}, \tag{6}$$

where i and j enumerate all the single-particle states of two adjacent configurations. In such a way, the original configuration at q can be tracked and the corresponding PES can be obtained as a function of the deformation [30].

In principle, if Δq is small enough, the configuration at $q+\Delta q$ should be the same as that at q. However, due to numerical difficulties, the condition in eq. (6) cannot be rigorously implemented. Therefore, the following procedures are adopted in our study: First, the wave function and occupation number of every state at the initial configuration q are recorded. Second, for each state i at configuration q, we search all the states of configuration $q+\Delta q$ for state j that has the largest overlap with state i. It is to be noted that state i and state j have the same quantum numbers Ω^π. Once state j is determined, the occupation number of state i will be transferred to state j. This procedure is repeated till the occupation number of each state at configuration $q+\Delta q$ is fixed. In cases that many single-particle states with the same symmetry are very close to each other, we adjust the step size of Δq to avoid the mismatch of the single-particle configuration.

3 Results and discussion

In the preceding section, we described how to implement the diabatic constrained method within the relativistic mean-field model. In this section, we would like to compare the results obtained with this method and those with the usual adiabatic constrained one. For this purpose, we study the potential energy surface of ^{208}Pb. This nucleus is chosen due to the following considerations: First, its properties can be well described by the RMF model; second, as a doubly magic nucleus, the pairing correlation can be safely ignored. The latter is particularly important because the pairing correlation can complicate the issue dramatically [24]. Taking into account the pairing correlation, such as using a constant gap pairing scheme, does not qualitatively alter our results and the corresponding conclusions. However, in the presence of the pairing correlation, due to the fractioned occupation number, it is not convenient to track configuration changes and discuss the relevant physics. Therefore, only the results without the pairing correlation are presented. It should be mentioned that the parameter set used is PK1, which has been carefully adjusted to reproduce both the nuclear-matter saturation properties and the ground-state properties of finite nuclei with a microscopic recipe for the center-of-mass correction [31].

In fig. 1, the PES of ^{208}Pb obtained from adiabatic (open circle) and diabatic (solid line) calculations are plotted as functions of the deformation parameter β_2. Surprisingly, it is found that even for ^{208}Pb, which has a rigid

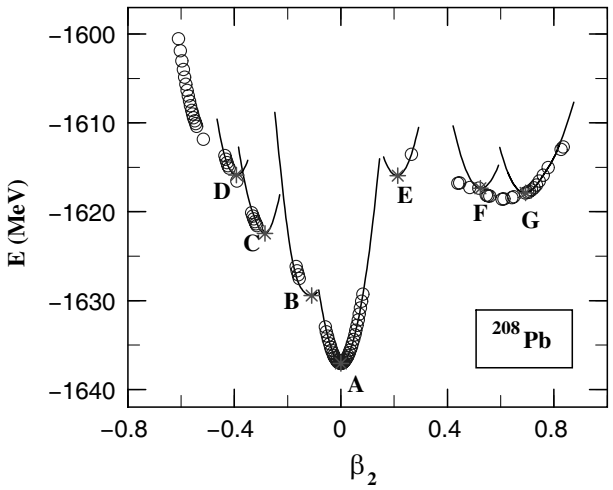

Fig. 1. (Color online) Potential energy surfaces of ^{208}Pb obtained in adiabatic (open circles) and diabatic calculations (solid lines). The local minima on the corresponding diabatic PES are denoted as stars and labelled by different capital letters, whose configuration, binding energy and deformation are tabulated in table 1.

spherical shape at the ground state, the adiabatic PES is somewhat complicated, which can be easily seen from the many broken regions on the PES. The fact that there exists an un-converged region on the adiabatic PES has been known for a long time. Over the years, it has been argued that it might originate from i) the abrupt change of configuration at a certain point due to the no crossing rule [29]; ii) change of the mean fields due to varied configuration [30]; and/or iii) the increased mixing of all low-lying states due to their near degeneracy [32]. On the other hand, the diabatic method is known to be able to connect broken regions existing in the adiabatic method. This can be clearly seen in fig. 1. In addition, from fig. 1, as expected, one can see that the diabatic results (solid lines) can reproduce the adiabatic results (open circles) very well if they both exist at the same region.

It should be noted that several local minima which do not exist on the adiabatic PES appear on the diabatic one. These minima, which could be viewed as excited states, are denoted as stars and labelled by capital letters in fig. 1. Since in the diabatic method, the single-particle levels of each configuration can be unambiguously determined (see the preceding section), we tabulate the corresponding configuration of each new local minimum in table 1. Each minimum is labelled by a bracket (E_x, β_2), where E_x is the excited energy relative to the ground state A and β_2 is the corresponding deformation parameter. The configuration of each state is given with respect to its core listed in the second row of the table. The configuration of state F relative to that of state E is not given simply because the difference between these two configurations is too large to fit into the table. We would like to point out a few more interesting things:

– From table 1, it is seen that for most cases both neutrons and protons are excited as configuration changes

Table 1. Configurations of the five local minima (B, C, D, E, G) on the diabatic potential energy surfaces of ^{208}Pb (see also fig. 1). Each minimum is labelled by a bracket (E_x, β_2) where E_x is the excited energy relative to the ground state A and β_2 the corresponding deformation parameter. The configuration of each state is relative to the core as listed in the second column.

State	Core	Configuration	
		π	ν
B $(7.63, -0.11)$	A	$(3s_{1/2})^{-1}(1h_{9/2})^{1}$	$(3p_{1/2})^{-1}(1i_{11/2})^{1}$
C $(15.63, -0.28)$	B	$(2d_{3/2})^{-2}(1i_{13/2})^{1}(2f_{7/2})^{1}$	$(3p_{3/2})^{-2}(2g_{9/2})^{1}(1j_{15/2})^{1}$
D $(21.19, -0.39)$	C		$(2f_{5/2})^{-3}(2h_{9/2})^{2}(1j_{13/2})^{1}$
E $(21.13, 0.21)$	A	$(3s_{1/2})^{-1}(2d_{3/2})^{-1}(1h_{9/2})^{2}$	$(3p_{1/2})^{-1}(2f_{5/2})^{-2}(2g_{9/2})^{2}(1i_{11/2})^{1}$
G $(19.19, 0.69)$	F	$(1g_{7/2})^{-1}(1h_{11/2})^{-1}(1h_{9/2})^{1}(1i_{13/2})^{1}$	$(3p_{3/2})^{-1}(2f_{7/2})^{-1}(1i_{11/2})^{1}(1j_{15/2})^{1}$

from one to the neighboring excited state. This might be related to the strong interaction between neutrons and protons. In this sense, a self-consistent calculation, such as the present one, is important to take care of this interaction and yields reliable results.

– Due to the fact that different local minima have different configurations, even the barrier between them is very small, they can still be well defined, such as B and A, F and G [21].

In fig. 1, the diabatic potential (solid curve) in fig. 1 show discontinuity around the deformations $\beta \sim 0.4$, which is due to the absence of the other diabatic curves with different configurations. If more careful diabatic constrained calculations with these configurations were done, the diabatic curves would become continuous and the two values at some quadrupole deformations, *e.g.*, $\beta \sim 0.4$, would belong to one or two of these diabatic curves.

To provide a microscopic explanation of fig. 1, we plot the single-particle spectra of ^{208}Pb near the Fermi level obtained from the diabatic calculation in fig. 2. Solid (dot-dashed) lines represent positive (negative) parity, filled (open) circles label the occupied (unoccupied) states, and the original configuration is that of the spherical case A (see fig. 1). The level crossing regions are highlighted by rectangles. From the top panel of fig. 2, one can easily see those high-j levels originating from $1h_{9/2}$ come down while those low-j levels, such as $3s_{1/2}$ and $2d_{3/2}$, go up as the nucleus becomes more oblate. At around $\beta_2 \approx -0.1$, the first level crossing happens between $3s_{1/2}$ and one $1h_{9/2}$ state. The same is true for neutrons, in particular, the first level crossing happens between $3p_{1/2}$ and one $1i_{11/2}$ state at $|\beta_2|$ slightly larger than that where the first proton level crossing occurs. It shows that a diabatic calculation is important to obtain the smooth evolution of the single-particle levels as a function of deformation. Otherwise irregularity of the single-particle levels will appear due to the occupation of the lower orbits in the adiabatic calculation. We should point out that here proton and neutron level crossings occur almost simultaneously mainly due to the fact that their corresponding Fermi levels are close to each other in the case of ^{208}Pb. It may not be the case for either proton- or neutron-rich nuclei where the proton and neutron Fermi surfaces are quite different. Beyond the crossing points, high-j levels continue coming down while low-j levels continue going up, which results in a very steep potential energy surface. This is the case for most diabatic PESs displayed in fig. 1.

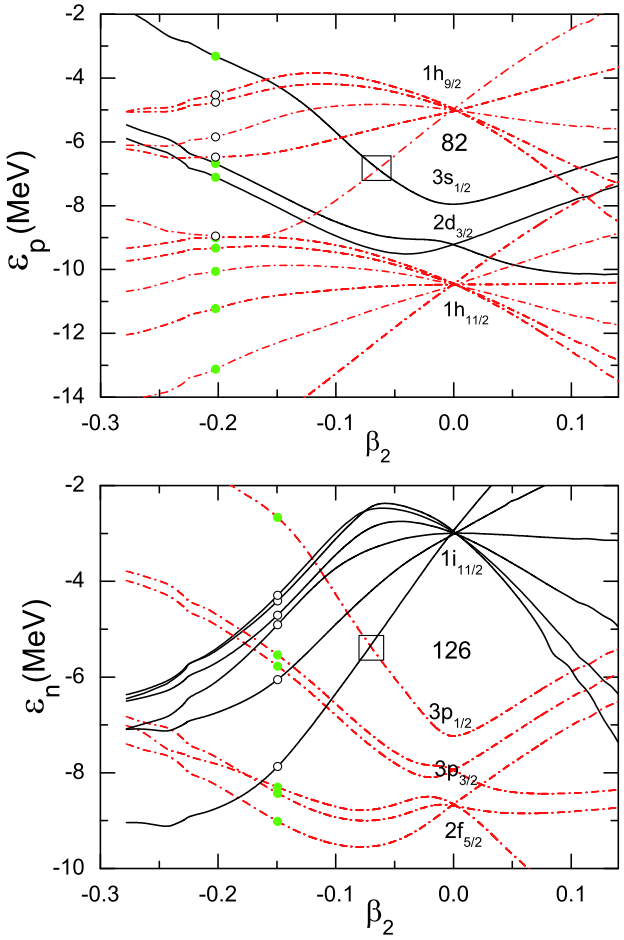

Fig. 2. (Color online) Proton (top panel) and neutron (bottom panel) single-particle states of ^{208}Pb obtained in diabatic calculations as functions of the deformation parameter β_2. The solid lines and the dot-dashed lines represent positive- and negative-parity states, respectively. The filled (open) circle denotes whether the corresponding state is occupied (unoccupied). The original configuration is that of the ground state. For the sake of clarity, only those states near the fermi surface are shown; and the level crossing points are highlighted by rectangles.

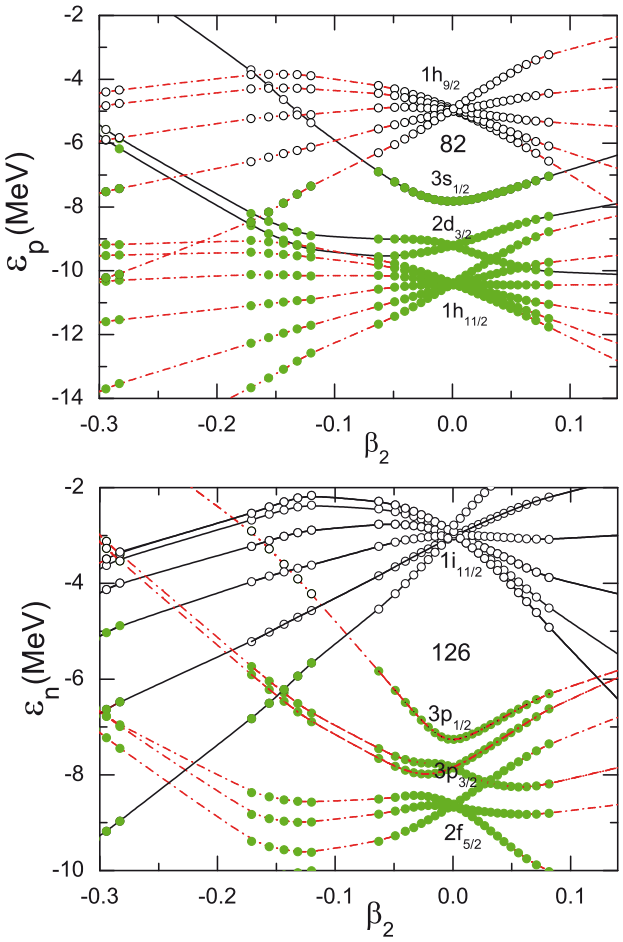

Fig. 3. (Color online) Proton (top panel) and neutron (bottom panel) single-particle states of ^{208}Pb obtained in adiabatic calculations as functions of the deformation parameter β_2. Lines and symbols as in fig. 2.

Finally, we plot the adiabatic single-particle levels in fig. 3. They look similar to those shown in fig. 2 but differ in two aspects. First, the diabatic single-particle levels are continuously distributed as functions of β_2 but the adiabatic single-particle levels are not. Their broken pattern is the same as that of the adiabatic PES shown in fig. 1. The underlying reason is, as we have mentioned above, that the sudden jump of the adiabatic PES is mostly due to the abrupt change of the corresponding configuration [30]. For example, the crossing of $3p_{1/2}$ and $1i_{11/2}$ at $\beta_2 \approx -0.1$ results in the broken PES shown in fig. 1. Second, the diabatic single-particle levels are occupied according to the dictated configuration but the adiabatic single-particle levels are so occupied to give the largest binding energy.

4 Summary

A diabatic constrained relativistic mean-field approach is proposed to calculate the potential energy surface of the nucleus and applied to ^{208}Pb. Although both adiabatic and diabatic constrained calculations yield almost the same ground-state PES, the diabatic one has the advantages that it enables one i) to decompose the segmented PES obtained in usual adiabatic approaches into separate parts characterized uniquely by different configurations; and ii) to define the single-particle orbits at each deformation by their quantum numbers unambiguously determined from their counterparts at the spherical configuration. Thus, the physics behind the adiabatic PES can be understood more clearly in the diabatic picture.

This work is partly supported by the National Natural Science Foundation of China under Grant Nos. 10435010, 10221003, and 10447101, and by the Doctoral Program Foundation from the Ministry of Education in China.

References

1. B.D. Serot, J.D. Walecka, Adv. Nucl. Phys. **16**, 1 (1986).
2. P.-G. Reinhard, Rep. Prog. Phys. **52**, 439 (1989).
3. P. Ring, Prog. Part. Nucl. Phys. **37**, 193 (1996).
4. J. Meng, P. Ring, Phys. Rev. Lett. **77**, 3963 (1996).
5. J. Meng, P. Ring, Phys. Rev. Lett. **80**, 460 (1998).
6. N.K. Glendenning, *Compact Stars* (Springer-Verlag, New York, 2000).
7. J. König, P. Ring, Phys. Rev. Lett. **71**, 3079 (1993).
8. J. Meng, H. Toki, J.Y. Zeng, S.Q. Zhang, S.G. Zhou, Phys. Rev. C **65**, R041302 (2002).
9. A. Arima, M. Harvey, K. Shimizu, Phys. Lett. B **30**, 517 (1969).
10. K.T. Hecht, A. Adler, Nucl. Phys. A **137**, 129 (1969).
11. J.N. Ginocchio, Phys. Rev. Lett. **78**, 436 (1997).
12. J. Meng, K. Sugawara-Tanabe, S. Yamaji, P. Ring, A. Arima, Phys. Rev. C **58**, R628 (1998).
13. J. Meng, K. Sugawara-Tanabe, S. Yamaji, A. Arima, Phys. Rev. C **59**, 154 (1999).
14. S.G. Zhou, J. Meng, P. Ring, Phys. Rev. Lett. **91**, 262501 (2003).
15. H. Madokoro, J. Meng, M. Matsuzaki, S. Yamaji, Phys. Rev. C **62**, 061301 (2000).
16. Z.Y. Ma, A. Wandelt, N.V. Giai, D. Vretenar, P. Ring, L.G. Cao, Nucl. Phys. A **703**, 222 (2002).
17. L.S. Geng, H. Toki, J. Meng, Prog. Theor. Phys. **113**, 785 (2005).
18. D. Vretenar, A.V. Afanasjev, G.A. Lalazissis, P. Ring, Phys. Rep. **409**, 101 (2005).
19. J. Meng, H. Toki, S.G. Zhou, S.Q. Zhang, W.H. Long, L.S. Geng, Prog. Part. Nucl. Phys. **57**, 470 (2005).
20. H. Flocard, P. Quentin, D. Vautherin, M. Véneroni, A.K. Kerman, Nucl. Phys. A **231**, 176 (1974).
21. R. Bengtsson, W. Nazarewicz, Z. Phys. A **334**, 269 (1989).
22. J. Meng, J.Y. Zeng, E.G. Zhao, High. En. Nucl. Phys. **18**, 249 (1994).
23. F.R. Xu, P.M. Walker, J.A. Sheikh, R. Wyss, Phys. Lett. B **435**, 257 (1998).
24. L. Guo, F. Sakata, E.G. Zhao, Commun. Theor. Phys. **41**, 257 (2004); L. Guo, F. Sakata, E.G. Zhao, Nucl. Phys. A **740**, 59 (2004).
25. A. Diaz-Torres, W. Scheid, Nucl. Phys. A **757**, 373 (2005).
26. S. Ĉwiok, P.-H. Heenen, W. Nazarewicz, Nature **433**, 705 (2005) and references therein.

27. F.R. May, V.V. Pashkevich, S. Frauendorf, Phys. Lett. B **68**, 113 (1977).
28. P. Ring, Y.K. Gambhir, G.A. Lalazissis, Comput. Phys. Commun. **105**, 77 (1997).
29. P. Ring, P. Schuck, *The Nuclear Many-body Problem* (Springer-Verlag, New York, 1980).
30. L. Guo, F. Sakata, E.G. Zhao, Phys. Rev. C **71**, 024315 (2005).
31. W.H. Long, J. Meng, N. Van Giai, S.-G. Zhou, Phys. Rev. C **69**, 034319 (2004).
32. M. Bender, P. Bonche, T. Duguet, P.-H. Heenen, Phys. Rev. C **69**, 064303 (2004).